



Cascade coherence transfer and magneto-optical resonances at 455 nm excitation of cesium

M. Auzinsh^a, R. Ferber^a, F. Gahbauer^{a,*}, A. Jarmola^a, L. Kalvans^a, A. Atvars^b

^a The University of Latvia, Laser Centre, Rainis Blvd., LV-1586 Riga, Latvia

^b Institute of Physical Research and Biomechanics, Maskavas Str. 22-1, LV-4604 Rezekne, Latvia

ARTICLE INFO

Article history:

Received 17 December 2010

Received in revised form 27 January 2011

Accepted 29 January 2011

Available online 20 February 2011

Keywords:

Cascade transitions

Ground-state Hanle effect

Bright and dark resonances

ABSTRACT

We present an experimental and theoretical study of nonlinear magneto-optical resonances observed in the fluorescence to the ground state from the $7P_{3/2}$ state of cesium, which was populated directly by laser radiation at 455 nm, and from the $6P_{1/2}$ and $6P_{3/2}$ states, which were populated via cascade transitions that started from the $7P_{3/2}$ state and passed through various intermediate states. The laser-induced fluorescence (LIF) was observed as the magnetic field was scanned through zero. Signals were recorded for the two orthogonal, linearly polarized components of the LIF. We compared the measured signals with the results of calculations from a model that was based on the optical Bloch equations and averaged over the Doppler profile. The calculations agree quite well with the measurements, especially when taking into account the fact that some experimental parameters were only estimated in the model.

© 2011 Elsevier B.V. All rights reserved.

1. Introduction

The technique of populating atomic states via cascade transitions from higher-lying states has been used for many years to study atomic properties and quantum phenomena. The excited-state Hanle effect, or zero-field level crossing in the case of weak excitation, has been used to measure lifetimes and hyperfine structure (hfs) parameters of atomic states. For example, Tsukakoshi and Shimoda [1] and Carrington [2] used discharge lamps to observe the cascade Hanle effect in order to study decay times of atomic levels in xenon and neon, respectively. The cascade Hanle effect has been used to study lifetimes of alkali metal S states [3] and, together with other cascade techniques, to measure lifetimes and hfs parameters of atomic states in alkali metal D states [4]. In some cases, the motivation for populating states via cascade transitions was to populate states that were otherwise unreachable via direct excitation [5,6]. Meanwhile, the ground-state Hanle effect was first observed by Lehmann and Cohen-Tannoudji [7]. Schmieder et al. [8] and later Alzetta et al. [9] observed dark resonances, where the fluorescence is at a minimum at zero magnetic field, when exciting D_1 or D_2 transitions in alkali metal atoms by means of discharge lamps. Similar resonances were observed by means of laser excitation by Ducloy et al. [10] in fluorescence signals and Gawlik et al. [11] in connection with the nonlinear Faraday effect. Much later, Dancheva et al. [12] observed bright resonances, which have a fluorescence maximum at zero magnetic field, in the D_1 and D_2 transitions of rubidium atoms in a

vapor cell. Recently, Gozzini and co-workers observed the narrow magneto-optical resonances associated with the ground-state Hanle effect in the fluorescence from states that were populated by cascade transitions from higher-lying states [13]. They excited the second resonance line of potassium with linearly and circularly polarized light and observed nonlinear magneto-optical resonances in the unpolarized fluorescence from the $4P_{1/2}$ and $4P_{3/2}$ transitions, which had been populated from the $5P_{3/2}$ state via spontaneous cascade transitions through various intermediate states. Measurements were obtained at various temperatures, but no theoretical description was given.

In the present article, we describe an experimental study of nonlinear magneto-optical resonances observed in the fluorescence to the ground-state via various de-excitation pathways from the $7P_{3/2}$ state (second resonance line) of cesium together with theoretical calculations to describe the observed signals. In addition, we monitor the transfer of coherence through these cascades by measuring the polarization degree of the fluorescence radiation, observed after excitation with linearly polarized radiation, and compare these measurements with theoretical calculations. Observations of nonlinear magneto-optical resonances in the fluorescence from states that are populated via cascades could be particularly interesting for magnetometry, because the resonances are narrow and can be observed at a wavelength far removed from the wavelength of the exciting laser radiation, which is the main source of noise in such measurements. Therefore, it seemed important to be able to study a system both experimentally and theoretically.

The basic theory of the fluorescence from a state populated from above via cascade transitions to a state other than the ground state was given by Gupta et al. [14] for linear excitation. The theory was

* Corresponding author. Tel.: +371 6 703 3790; fax: +371 6 703 3751.

E-mail address: florian.gahbauer@lu.lv (F. Gahbauer).

based on the optical Bloch equations for the density matrix. In 1978 Picqué used the optical Bloch equations to describe accurately dark resonances that arose in nonlinear excitation of one hyperfine component of the D_1 transition in a strongly excited beam of sodium atoms [15]. In recent years, such models have achieved very good agreement for the D_1 transitions of cesium [16] and rubidium [17] when averaging over the Doppler profile and taking into account the coherence properties of the laser radiation, as well as all adjacent hyperfine states and even the small effect of the mixing of magnetic sublevels in the magnetic field.

In the context of the present study it was necessary to adapt the theoretical model developed for magneto-optical resonances in the D lines of alkali metal atoms under nonlinear excitation in Refs. [16,17] to the cascade transitions that result when the second resonance line of alkali atoms was excited. We compared experimentally measured signals with the results of calculations of the intensity of direct fluorescence from the $7P_{3/2}$ state of cesium, as well as fluorescence from the $6P_{3/2}$ state (D_2 line) and the $6P_{1/2}$ state (D_1 line). The calculations were based on an extension of a theoretical model developed for the first resonance line of alkali metal atoms. However, in the case of cascade transitions, the large number of decay channels leads to a density matrix that is substantially larger than in the case for the first resonance line. We studied the unpolarized fluorescence intensity emitted along the direction of the scanned magnetic field as well as the polarized fluorescence intensity and the polarization degree. Fig. 1 shows the atomic states involved in our experiment. The figure includes the exciting line, the cascade pathways, and the observed fluorescence lines. The theoretical model took into account the population and coherence transfer of all possible de-excitation paths. As a result, it was necessary to solve very large systems of equations, which is computationally intensive and, thus, time-consuming. Therefore, instead of searching for the optimal parameters needed to describe the experimental signals in detail, we aimed to reproduce and understand the experimental features using estimated values for the model parameters.

2. Experimental description

In the experiment, a Toptica TA-SHG110 laser at 455 nm was used to excite cesium atoms in a vapor cell. The cell was home-made and kept at room temperature at the center of a three-axis Helmholtz coil system. Two sets of coils were used to cancel the ambient magnetic field, while the third set was used to scan the magnetic field B from -7 G to $+7$ G by means of a Kepco BOP-50-8M bipolar power supply. The laser was usually tuned to the frequency for which the

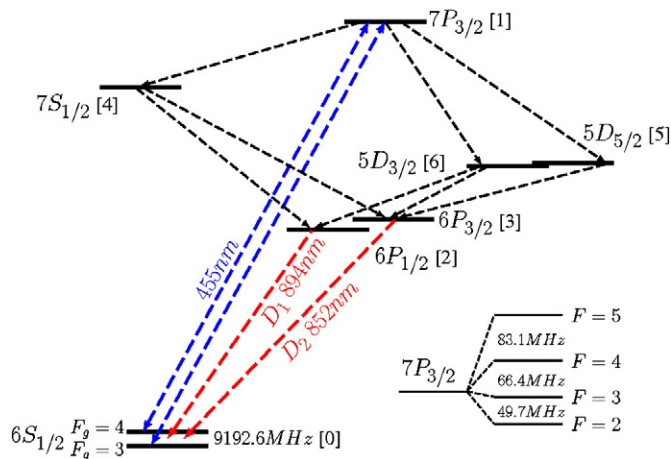


Fig. 1. Level diagram. Excitation takes place at 455 nm. Fluorescence is observed at 455 nm, 894 nm, and 852 nm. The numbers in square brackets correspond to the labeling scheme used in the equations of Section 3.2.

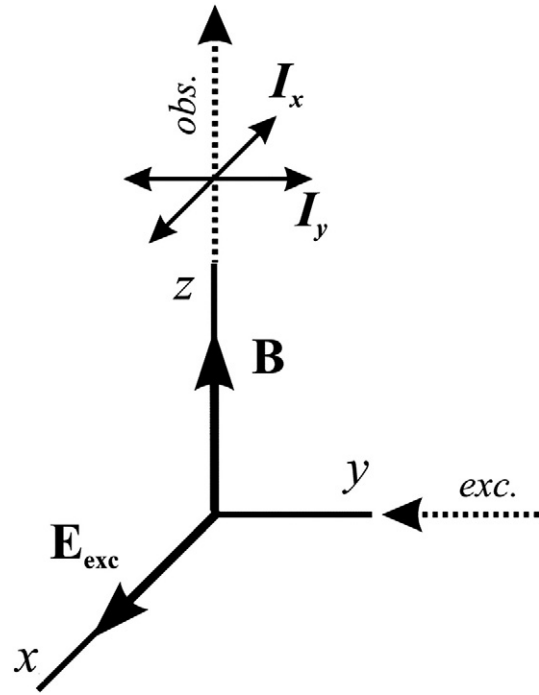


Fig. 2. Experimental geometry. The relative orientation of the laser beam (*exc.*), laser light polarization (E_{exc}), magnetic field (B), and observation direction (*obs.*) are shown. I_x and I_y are the linearly polarized components of the LIF intensity.

fluorescence at zero magnetic field was at a maximum for a given transition, except in the case of certain studies where it was deliberately detuned from this frequency by a known amount. The laser frequency was monitored using a High-Finesse WS7 wavemeter to ensure that the frequency did not drift significantly during an experiment. During a given measurement, the laser frequency did not drift by more than 10 MHz.

The geometry of the polarization vector of the exciting laser radiation, the magnetic field, and the direction of fluorescence observation are given in Fig. 2. The fluorescence light was focused with a lens onto a polarizing beam splitter, which directed two orthogonally polarized components of the fluorescence radiation to two separate photodiodes (Thorlabs FDS-100). In front of the polarizing beam-splitter, interference filters were used to select fluorescence at 455 nm, 852 nm, or 894 nm. Two different polarizing beam splitters were used, depending on the wavelength of the fluorescence radiation being observed: one was used for observations at 852 and 894 nm, while another was used for observations at 455 nm. The photodiode signals were amplified and recorded separately on an Agilent DSO5014A oscilloscope. To balance the amplifiers of the two photodiodes, the laser beam polarization was turned in such a way that the polarization vector of the laser radiation was parallel to the magnetic field. The difference signal ($I_x - I_y$) in this case should be zero when the amplifications of the photodiodes are properly balanced. Differences in sensitivity to unpolarized light and electronic offsets present in the absence of any light were also checked and taken into account.

The cross-section of the laser beam determines the transit relaxation rate, and it was 3.2 mm^2 . The beam cross-section was determined by considering the area of the beam where the power density was within 50% of the maximum power density. The beam profile, which was approximately circular, was characterized by means of a Thorlabs BP104-VIS beam profiler. Different powers were selected by means of neutral density filters. Unless otherwise specified, the results presented in this article were obtained with a laser beam whose cross-sectional area was 3.2 mm^2 and whose total laser power was 40 mW. For some experiments, diminished laser

powers were obtained using neutral density filters: 10 mW, 2.5 mW, and 0.625 mW.

The signal background was determined by tuning the laser away from the resonance. No additional background from scattered laser-induced fluorescence (LIF) was taken into account in the analysis.

3. Theoretical model

3.1. Outline of the model

In order to build a model of the nonlinear Hanle effect in alkali atoms confined to a cell, we used the density matrix of an atomic ensemble. The diagonal elements of the density matrix ρ_{ii} of an atomic ensemble describe the population of a certain atomic level i , and the non-diagonal elements ρ_{ij} describe coherences created between the levels i and j . In our particular case the levels in question are magnetic sublevels of a certain hfs level. If atoms are excited from the ground state hfs level g to the excited state hfs level e , then the density matrix consists of elements ρ_{g,g_j} and ρ_{e,e_j} , called Zeeman coherences, as well as “cross-elements” ρ_{g,e_j} , called optical coherences.

The time evolution of the density matrices is described by optical Bloch equations (OBEs), which can be written as [18,19]:

$$i\hbar \frac{\partial \rho}{\partial t} = [\hat{H}, \rho] + i\hbar \hat{R} \rho, \quad (1)$$

where the operator \hat{R} represents the relaxation matrix. If an atom interacts with laser light and an external dc magnetic field, the Hamiltonian can be expressed as $\hat{H} = \hat{H}_0 + \hat{H}_B + \hat{V}$. \hat{H}_0 is the unperturbed atomic Hamiltonian, which depends on the internal atomic coordinates, \hat{H}_B is the Hamiltonian of the atomic interaction with the magnetic field, and $\hat{V} = -\hat{d} \cdot \mathbf{E}(t)$ is the interaction operator with the oscillating electric field in the dipole approximation, where \hat{d} is the electric dipole operator and $\mathbf{E}(t)$, the electric field of the exciting light.

When using the OBEs to describe the interaction of alkali atoms with laser radiation in the presence of a dc magnetic field, we describe the light classically as a time dependent electric field of a definite polarization \mathbf{e} :

$$\mathbf{E}(t) = \varepsilon(t) \mathbf{e} + \varepsilon^*(t) \mathbf{e}^* \quad (2)$$

$$\varepsilon(t) = |\varepsilon_{\bar{\omega}}| e^{-i\Phi(t) - i(\bar{\omega} - \mathbf{k}_{\bar{\omega}} \cdot \mathbf{v})t}, \quad (3)$$

where $\bar{\omega}$ is the center frequency of the spectrum and $\Phi(t)$ is the fluctuating phase, which gives the spectrum a finite bandwidth. In this model the line shape of the exciting light is assumed to be Lorentzian with line-width $\Delta\omega$. As each atom moves with a particular velocity \mathbf{v} , it experiences a shift $\bar{\omega} - \mathbf{k}_{\bar{\omega}} \cdot \mathbf{v}$ in the laser frequency due to the Doppler effect, where $\mathbf{k}_{\bar{\omega}}$ is the wave vector of the exciting light. The treatment of the Doppler effect is described in Section 3.2.

The matrix elements of the dipole operator \hat{d} that couple the i sublevel with the j sublevel can be written as: $d_{ij} = \langle i | \hat{d} \cdot \mathbf{e} | j \rangle$. In the external magnetic field, sublevels are mixed so that each sublevel i with magnetic quantum number M labeled as ξ is a mixture of different hyperfine levels $|F M\rangle$ with mixing coefficients $C_{i,F,M}$:

$$|i\rangle = |\xi M\rangle = \sum_F C_{i,F,M} |FM\rangle. \quad (4)$$

The mixing coefficients $C_{i,F,M}$ are obtained as the eigenvectors of the Hamiltonian matrix of a fine structure state in the external magnetic field. Since some of the upper states in the cascade system have rather small hyperfine splittings, the mixing of magnetic sublevels can be rather significant. For example, at a magnetic field of 7 G, the mixing coefficients for the $7P_{3/2}$ state are on the order of 10%, while in the $5D_{3/2}$ state the magnetic sublevels are fully mixed.

The dipole transition matrix elements $\langle F_k M_k | \hat{d} \cdot \mathbf{e} | F_l M_l \rangle$ should be expanded further using angular momentum algebra, including the Wigner–Eckart theorem and the fact that the dipole operator acts only on the electronic part of the hyperfine state, which consists of electronic and nuclear angular momentum (see, for example, Refs. [19,20]).

3.2. Rate equations

The rate equations for Zeeman coherences are developed by applying the rotating wave approximation to the optical Bloch equations with an adiabatic elimination procedure for the optical coherences [18] and then accounting realistically for the fluctuating laser radiation by taking statistical averages over the fluctuating light field phase (*the decorrelation approximation*) and assuming a specific phase fluctuation model: random phase jumps or continuous random phase diffusion. As a result we arrive at the rate equations for Zeeman coherences for the ground and excited state sublevels of atoms [21]. In applying this approach to a case in which atoms are excited only in the finite region corresponding to the laser beam diameter, we have to take into account transit relaxation.

In Ref. [21], only resonant excitation at the D lines was considered with one ground state and one excited state. In the case of the cascade transitions considered here we have more than two states, and so they are denoted as follows (see Fig. 1): the $6S_{1/2}$ state is denoted by ‘[0]’ and the part of the density matrix related to this level is represented by $\rho^{[0]}$. The $7P_{3/2}$ state is denoted by ‘[1]’ and the part of the density matrix that corresponds to it as $\rho^{[1]}$. Similarly, the $6P_{1/2}$ state is indicated by ‘[2]’, the $6P_{3/2}$ state by ‘[3]’, the $7S_{1/2}$ state by ‘[4]’, the $5D_{5/2}$ state by ‘[5]’ and the $5D_{3/2}$ state by z ‘[6]’. If the above treatment of the OBEs is applied to the level scheme in discussion, we obtain the following rate equations:

$$\begin{aligned} \frac{\partial \rho_{g,g_j}^{[0]}}{\partial t} = & -i\omega_{g,g_j} \rho_{g,g_j}^{[0]} - \gamma \rho_{g,g_j}^{[0]} \\ & + \left(\sum_{e_k e_m} \Gamma_{[0]g_j g_j}^{[1]e_k e_m} \rho_{e_k e_m}^{[1]} + \sum_{e_k e_m} \Gamma_{[0]g_j g_j}^{[2]e_k e_m} \rho_{e_k e_m}^{[2]} + \sum_{e_k e_m} \Gamma_{[0]g_j g_j}^{[3]e_k e_m} \rho_{e_k e_m}^{[3]} \right) \\ & + \frac{|\varepsilon_{\bar{\omega}}|^2}{\hbar^2} \sum_{e_k e_m} \left(\frac{1}{\Gamma_R + i\Delta_{e_m g_j}} + \frac{1}{\Gamma_R - i\Delta_{e_k g_j}} \right) d_{g_i e_k}^* d_{e_m g_j} \rho_{e_k e_m}^{[1]} \\ & - \frac{|\varepsilon_{\bar{\omega}}|^2}{\hbar^2} \sum_{e_k g_m} \left(\frac{1}{\Gamma_R - i\Delta_{e_k g_j}} d_{g_i e_k}^* d_{e_k g_m} \rho_{g_m g_j}^{[0]} + \frac{1}{\Gamma_R + i\Delta_{e_k g_j}} d_{g_m e_k}^* d_{e_k g_j} \rho_{g_i g_m}^{[0]} \right) \\ & + \lambda \delta(g_i, g_j), \end{aligned} \quad (5)$$

$$\begin{aligned} \frac{\partial \rho_{e_i e_j}^{[1]}}{\partial t} = & -i\omega_{e_i e_j} \rho_{e_i e_j}^{[1]} - (\gamma + \Gamma^{[1]}) \rho_{e_i e_j}^{[1]} \\ & + (0) + \frac{|\varepsilon_{\bar{\omega}}|^2}{\hbar^2} \sum_{g_k, g_m} \left(\frac{1}{\Gamma_R - i\Delta_{e_i g_m}} + \frac{1}{\Gamma_R + i\Delta_{e_j g_k}} \right) d_{e_i g_k}^* d_{g_m e_j} \rho_{g_k g_m}^{[0]} \\ & - \frac{|\varepsilon_{\bar{\omega}}|^2}{\hbar^2} \sum_{g_k, e_m} \left(\frac{1}{\Gamma_R + i\Delta_{e_j g_k}} d_{e_i g_k}^* d_{g_k e_m} \rho_{e_m e_j}^{[1]} + \frac{1}{\Gamma_R - i\Delta_{e_i g_k}} d_{e_m g_k}^* d_{g_k e_j} \rho_{e_i e_m}^{[1]} \right), \end{aligned} \quad (6)$$

$$\begin{aligned} \frac{\partial \rho_{f_j f_j}^{[2]}}{\partial t} = & -i\omega_{f_j f_j} \rho_{f_j f_j}^{[2]} - (\gamma + \Gamma^{[2]}) \rho_{f_j f_j}^{[2]} \\ & + \left(\sum_{e_k e_m} \Gamma_{[2]f_j f_j}^{[4]e_k e_m} \rho_{e_k e_m}^{[4]} + \sum_{e_k e_m} \Gamma_{[2]f_j f_j}^{[6]e_k e_m} \rho_{e_k e_m}^{[6]} \right), \end{aligned} \quad (7)$$

$$\frac{\partial \rho_{f_i f_j}^{[3]}}{\partial t} = -i\omega_{f_i f_j} \rho_{f_i f_j}^{[3]} - (\gamma + \Gamma^{[3]}) \rho_{f_i f_j}^{[3]} + \left(\sum_{e_k e_m} \Gamma_{[3] f_i f_j}^{[4] e_k e_m} \rho_{e_k e_m}^{[4]} + \sum_{e_k e_m} \Gamma_{[3] f_i f_j}^{[5] e_k e_m} \rho_{e_k e_m}^{[5]} + \sum_{e_k e_m} \Gamma_{f_i f_j}^{[6] e_k e_m} \rho_{e_k e_m}^{[6]} \right), \quad (8)$$

$$\frac{\partial \rho_{f_i f_j}^{[4]}}{\partial t} = -i\omega_{f_i f_j} \rho_{f_i f_j}^{[4]} - (\gamma + \Gamma^{[4]}) \rho_{f_i f_j}^{[4]} + \sum_{e_k e_m} \Gamma_{[4] f_i f_j}^{[1] e_k e_m} \rho_{e_k e_m}^{[1]}, \quad (9)$$

$$\frac{\partial \rho_{f_i f_j}^{[5]}}{\partial t} = -i\omega_{f_i f_j} \rho_{f_i f_j}^{[5]} - (\gamma + \Gamma^{[5]}) \rho_{f_i f_j}^{[5]} + \sum_{e_k e_m} \Gamma_{[5] f_i f_j}^{[1] e_k e_m} \rho_{e_k e_m}^{[1]}, \quad (10)$$

$$\frac{\partial \rho_{f_i f_j}^{[6]}}{\partial t} = -i\omega_{f_i f_j} \rho_{f_i f_j}^{[6]} - (\gamma + \Gamma^{[6]}) \rho_{f_i f_j}^{[6]} + \sum_{e_k e_m} \Gamma_{[6] f_i f_j}^{[1] e_k e_m} \rho_{e_k e_m}^{[1]}. \quad (11)$$

Here g_i denotes the ground state '0' magnetic sublevel, while e_i and f_i denote magnetic sublevels of state '1', '2', '3', '4', '5', or '6' according to the associated index, with e_i always referring to the level with higher energy. For example, f_i in the expression $\rho_{f_i f_j}^{[5]}$ belongs to level '5'. The term, $\Delta_{ij} = \bar{\omega} - \mathbf{k}_{\bar{\omega}} \mathbf{v} - \omega_{ij}$ expresses the actual laser shift away from the resonance for transitions between levels $|i\rangle$ and $|j\rangle$ for atoms moving with velocity \mathbf{v} . The total relaxation rate Γ_R is given by $\Gamma_R = \frac{\Gamma^{[1]}}{2} + \frac{\Delta\omega}{2} + \gamma$, where $\Gamma^{[k]}$ is the relaxation rate of the level 'k', γ is the transit relaxation rate, and λ is the rate at which "fresh" atoms move into the interaction region. The rate γ can be estimated as $1/(2\pi\tau)$, where τ is time it takes for an atom to cross the laser beam at the mean thermal velocity v_{th} . It is assumed that the atomic equilibrium density outside the interaction region is normalized to 1, which leads to λ numerically equal to γ , since $\lambda = \gamma n_0$, where n_0 is the density of atoms. The term $\Gamma_{f_i f_j}^{e_i e_j}$ is the rate at which excited state population and coherences are transferred to the lower state as a result of spontaneous transitions and it is obtained as follows [19]:

$$\Gamma_{f_i f_j}^{e_i e_j} = \Gamma^s (-1)^{2F_e - M_{e_i} - M_{e_j}} (2F_f + 1) \sum_q \begin{pmatrix} F_e & 1 & F_f \\ -M_{e_i} & q & M_{f_j} \end{pmatrix} \begin{pmatrix} F_e & 1 & F_f \\ -M_{e_j} & q & M_{f_i} \end{pmatrix}. \quad (12)$$

If the system is closed, all excited state atoms return to the initial state through spontaneous transitions. Note that $\sum_{e_i f_j} \Gamma_{r|f_i f_j}^{[s] e_i e_j} = \alpha(s, r) \Gamma^{[s]}$ where $\alpha(s, r)$ is the branching ratio of spontaneous emission from level 's' to level 'r'. Furthermore, $\sum_r \alpha(s, r) = 1$.

Eqs. (5)–(11) describe the time evolution of the parts of the density matrix for states $[i] = [0]$ –[6], respectively. The first term on the right-hand side of each equation describes the destruction of the Zeeman coherences due to magnetic sublevel splitting in an external magnetic field $\omega_{ij} = (E_i - E_j)/\hbar$. The second term characterizes the effects of the transit relaxation rate ($\gamma^{[i]}$) and the spontaneous relaxation rate ($\Gamma^{[i]}$), with the latter being absent for the ground state '[0]'. The next term shows the transfer of population and coherences from the upper state $[j]$ to the state $[i]$ described by a particular equation due to spontaneous transitions; this term is equal to zero in Eq. (6), which describes the '[1]' level, as no levels above this one are excited. For Eqs. (5) and (6) the fourth term describes the population increase in the level due to laser-induced transitions, while the fifth term stands for the population driven away from the state via laser-induced transitions. Finally, the sixth term in Eq. (5) describes how the population of "fresh atoms" is supplied to the initial state from the volume outside the laser beam in a process of transit relaxation.

For a multilevel system that interacts with laser radiation, we can define the effective Rabi frequency in the form $\Omega = \frac{|k_{\bar{\omega}}|}{\hbar} \langle J_e || d || J_g \rangle$, where J_e is the angular momentum of the excited state '1' fine structure level, and J_g is the angular momentum of the ground state '0'

fine structure level. The influence of the magnetic field appears directly in the magnetic sublevel splitting ω_{ij} and indirectly in the mixing coefficients C_{i, F_k, M_i} and C_{j, F_l, M_j} of the dipole matrix elements d_{ij} .

We look at quasi-stationary excitation conditions so that $\partial \rho_{g_i g_j}^{[0]}/\partial t = \partial \rho_{e_i e_j}^{[1]}/\partial t = \partial \rho_{f_i f_j}^{[2]}/\partial t = \partial \rho_{f_i f_j}^{[3]}/\partial t = \partial \rho_{f_i f_j}^{[4]}/\partial t = \partial \rho_{f_i f_j}^{[5]}/\partial t = \partial \rho_{f_i f_j}^{[6]}/\partial t = 0$.

By solving the rate equations as an algebraic system of linear equations for $\rho_{g_i g_j}^{[0]}$ and $\rho_{e_i e_j}^{[1]}$, $\rho_{e_i e_j}^{[2]}$, $\rho_{e_i e_j}^{[3]}$, $\rho_{e_i e_j}^{[4]}$, $\rho_{e_i e_j}^{[5]}$ and $\rho_{e_i e_j}^{[6]}$ we obtain the matrix of populations and Zeeman coherences for all levels involved ('0'–'6'). This matrix allows us to obtain immediately the intensity of the observable fluorescence characterized by the polarization vector \mathbf{e} [19,20]. Fluorescence that is transmitted from the excited-state level 'i' to the ground-state level 'j' is obtained as:

$$I^{[i]}(\bar{\mathbf{e}}) = I_0^{[i]} \sum_{g_i, e_i, e_j} d_{g_i e_i}^{(ob)*} d_{e_i g_i}^{(ob)} \rho_{e_i e_j}^{[i]}, \quad (13)$$

where $I_0^{[i]}$ is a proportionality coefficient. The dipole transition matrix elements $d_{e_i g_j}^{(ob)}$ characterize the dipole transition from the excited state e_i to some ground state g_j for the transition on which the fluorescence is observed.

To calculate the fluorescence produced by an ensemble of atoms, we have to treat the previously written expression for the fluorescence as a function of both the polarization vector of the fluorescence and the atomic velocity, $I^{[i]}(\bar{\mathbf{e}}) = I^{[i]}(\bar{\mathbf{e}}, \mathbf{k}_{\bar{\omega}} \mathbf{v})$ and average it over the Doppler profile while taking into account the different velocity groups $\mathbf{k}_{\bar{\omega}} \mathbf{v}$ with their respective statistical weights. If the unpolarized fluorescence without discrimination of the polarization or frequency is recorded, one needs to sum the fluorescence over the two orthogonal polarization components and all possible final state hfs levels.

3.3. Model parameters

In order to perform theoretical simulations with the methods described in the previous section, a number of theoretical parameters and atomic constants had to be used. Some parameters are known rather precisely. Thus, the hyperfine splitting constants for atomic levels involved in the cesium D lines were obtained from Ref. [22], while the magnetic dipole and electric quadrupole constants for the remaining energy levels were taken from Ref. [23]. The natural linewidths for levels not involved in the D lines were obtained from Ref. [24]. The branching ratios for the cascade transitions are available from the NIST database [25,26] and in Ref. [27].

For the parameters that were related to the experimental conditions, we used reasonable estimates based on measurements of the laser beam parameters and our previous experience. The transit relaxation rate is the inverse of the mean time that an atom spends in the laser beam as it moves chaotically in the vapor cell with a thermal velocity. For a laser beam diameter of 2 mm (full width at half maximum of the intensity profile) and room temperature (293 K), we used a value of 0.02 MHz. To estimate the Rabi frequency to be used in the simulations, we calculated the saturating laser power density for the excitation transition using its natural linewidth and then related this value to the power densities used in the experiments. The saturating laser power density is the laser power density at which the stimulated emission equals the spontaneous decay rate, and it can be obtained from the formula [28]:

$$I_{sat} = \frac{4\hbar c \Omega_{sat}^2}{\lambda_{eg}^3 \Gamma^{[1]}}. \quad (14)$$

In such a way the saturating Rabi frequency Ω_{sat} in our experiment was estimated to be about 5 MHz. In the calculations, the results were

averaged over the Doppler profile with the appropriate weighting factor and a step-size of 2.5 MHz. Another parameter that had to be estimated was the laser frequency. For the experiment, the reference frequency for a given transition was the frequency at which maximum fluorescence was observed.

4. Results and discussion

Both orthogonal, linearly polarized polarization components $I_{x,y}$ were recorded in all experiments. To visualize the data, three quantities were considered: the unpolarized fluorescence ($I_x + I_y$), the polarized fluorescence (I_x and I_y), and the polarization degree $[(I_x - I_y)/(I_x + I_y)]$.

4.1. Unpolarized fluorescence

Fig. 3 displays results obtained by exciting the $7P_{3/2}$ state from the $F_g = 3$ ground-state level and observing direct, unpolarized fluorescence to the ground state from the $7P_{3/2}$ state as well as fluorescence to the ground state from the $6P_{3/2}$ (D_2 line) and $6P_{1/2}$ (D_1 line) states, which had been populated by cascade transitions. In all cases, a narrow, dark, Hanle-type resonance was observed. The experiment showed, and theoretical calculations confirmed, that the shape of the resonance does not depend on which fluorescence line to the ground state is observed [see Fig. 3(a) and Fig. 3(b)]. In fact, the three experimental curves in Fig. 3(a) are practically indistinguishable, and the same is true for the three theoretical curves in Fig. 3(b). Fig. 3(c)

shows the unpolarized fluorescence intensity observed from the $6P_{1/2}$ state populated via cascades versus magnetic field. Experimental measurements and results from calculations are shown on the same plot. Because the calculations are extremely time-consuming, it was not possible to vary the model parameters in order to find those experimental parameters that could not be measured directly. Nevertheless, by making reasonable estimates of the parameter values based on the experience gained in Refs. [16,17], it was possible to obtain almost perfect agreement between experiment and theory (see Section 3.3). The theoretical calculation assumed that the laser frequency was tuned to the $F_g = 3 \rightarrow F_e = 3$ transition.

Fig. 3(d) shows the measured resonance contrasts for each observed fluorescence line as a function of laser power density. Similar to the case of nonlinear magneto-optical resonances in D line excitation, the contrast increased with increasing laser power density up to some maximum and then decreased (see, for example, Fig. 8 in Ref. [17]).

Fig. 4 shows similar results as Fig. 3, except that in Fig. 4, the atoms were excited from the $F_g = 4$ ground-state level. One notable difference with the case of excitation from the $F_g = 3$ level is that the resonance shapes did depend on which fluorescence line was observed [see Fig. 4(a)]. The theoretical calculations in Fig. 4(b) confirm that the resonance shape, in particular the contrast, depends on the fluorescence line that is observed. The theoretical calculations do not reproduce the experimental signals extremely well at fields larger than several Gauss. However, the theoretical curve in Fig. 4(c) describes quite well the narrow portion of the resonance up to a magnetic field of up to about

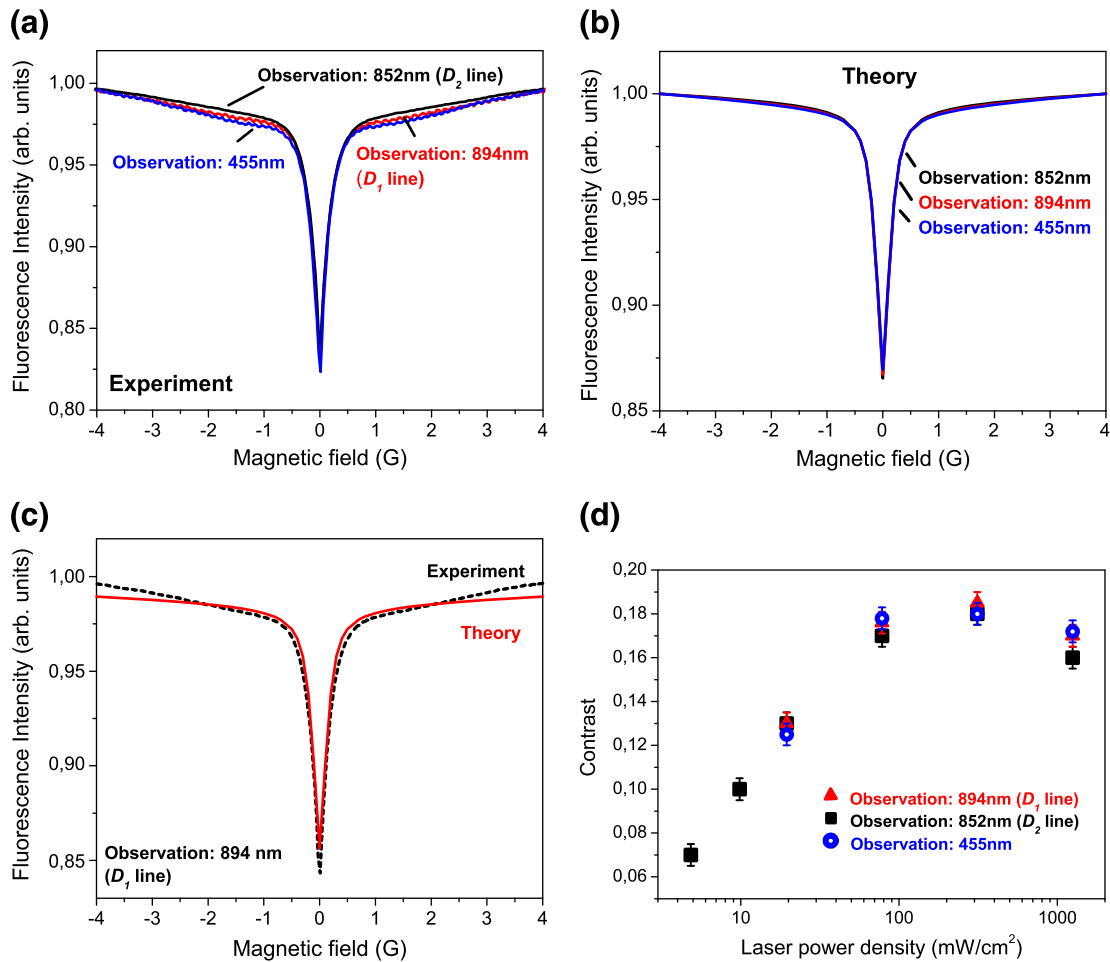


Fig. 3. Intensity of the non-polarized fluorescence to the ground state versus magnetic field for excitation of the $6S_{1/2}(F_g = 3) \rightarrow 7P_{3/2}$ transition at 455 nm. (a) Observed fluorescence from the $7P_{3/2}$ (direct), $6P_{3/2}$ (cascade), and $6P_{1/2}$ (cascade) states. The three curves are practically indistinguishable. (b) Theoretical calculations corresponding to the observations in (a). The three curves almost coincide. (c) Experimental observation and theoretical calculation of the fluorescence from the $6P_{1/2}$ state (D_1 transition). (d) Observed contrast as a function of the laser power density for the fluorescence from the three levels mentioned in (a).

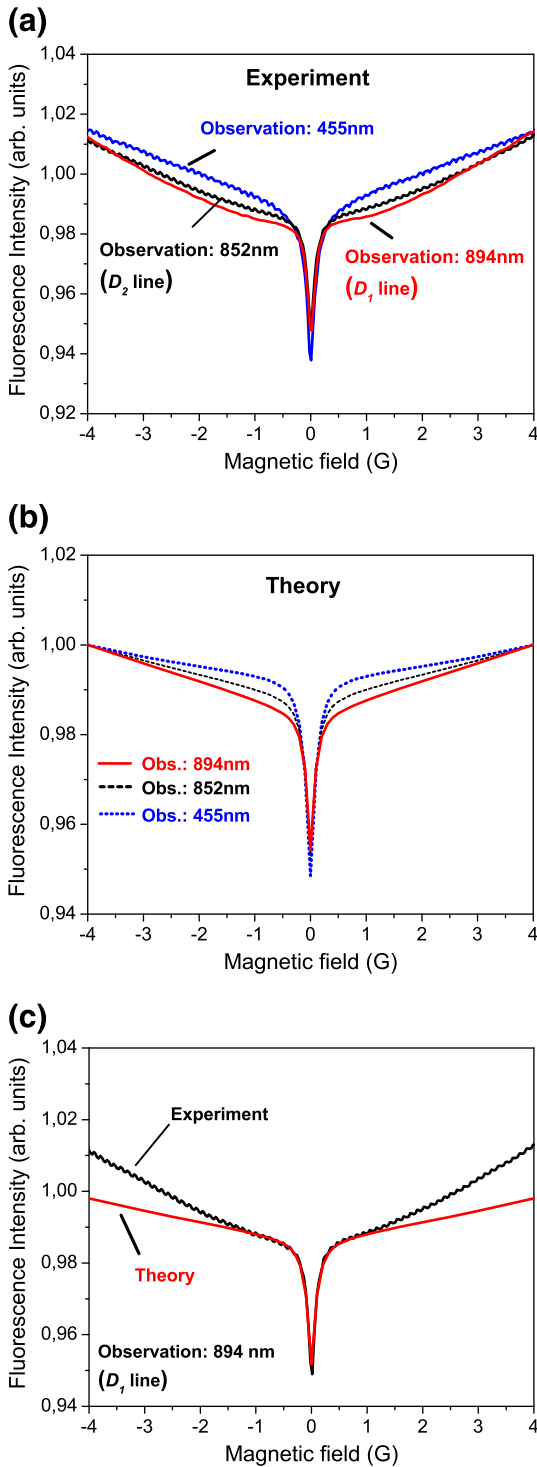


Fig. 4. Intensity of the non-polarized fluorescence to the ground state versus the magnetic field for excitation of the $6S_{1/2}(F_g=4) \rightarrow 7P_{3/2}$ transition at 455 nm. (a) Observed fluorescence from the $7P_{3/2}$ (direct), $6P_{3/2}$ (cascade), and $6P_{1/2}$ (cascade) states. (b) Theoretical calculations corresponding to the observations in (a). (c) Experimental observation and theoretical calculation of the fluorescence from the $6P_{1/2}$ state (D_1 transition).

± 1 G. For the purpose of modeling the transition, we assumed that the laser was tuned to the $F_g=4 \rightarrow F_e=4$ transition.

4.2. Polarized fluorescence

Fig. 5 depicts as a function of magnetic field the intensities of two orthogonally polarized fluorescence components from the de-excitation

of the $7P_{3/2}$ state directly to the ground state for various values of the laser detuning. The value of zero detuning in Fig. 5(a) was chosen to correspond to the frequency at which the value of the observed

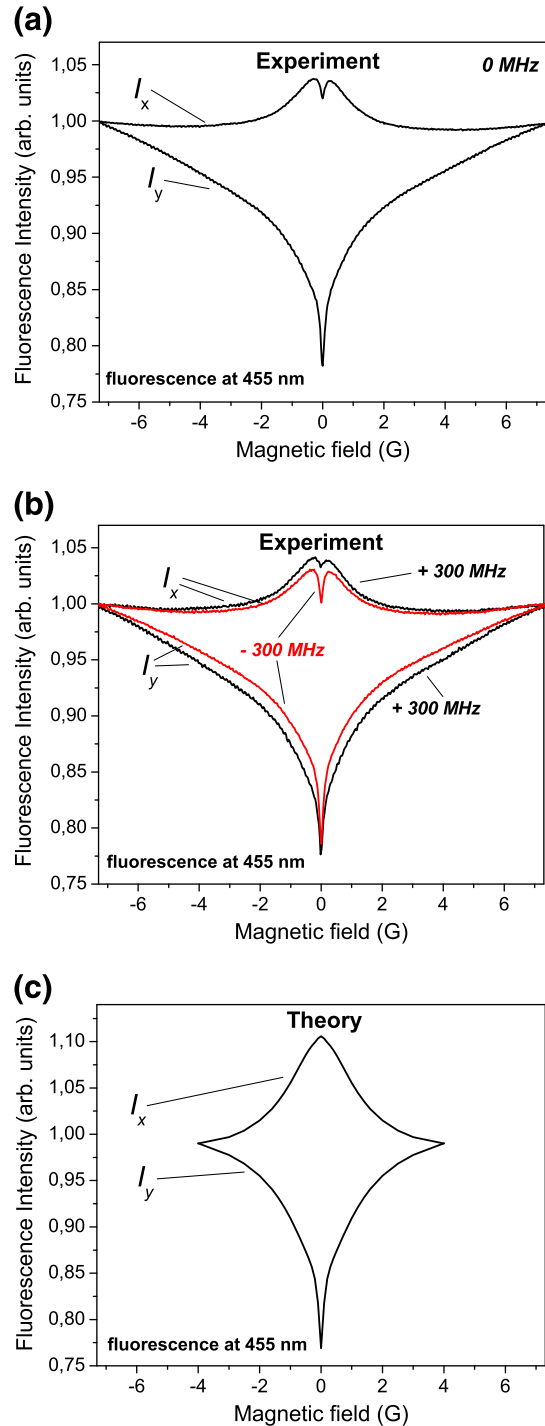


Fig. 5. Intensities of the orthogonally polarized components I_x and I_y of the fluorescence from the $7P_{3/2}$ state to the ground state versus the magnetic field for excitation from the $F_g=4$ ground-state level for various laser detunings from the frequency of maximum observed fluorescence intensity. The intensities of the fluorescence with polarization vector parallel or perpendicular to the polarization vector of the exciting laser radiation are denoted as I_x and I_y , respectively (see Fig. 2). (a) Observations with the exciting laser (455 nm) tuned to the frequency that gave maximum fluorescence (0 detuning). (b) Observations with the exciting laser detuned by ± 300 MHz from the frequency at which the observed fluorescence intensity was at a maximum. (c) Theoretical calculations for the laser tuned exactly to the $F_g=4 \rightarrow F_e=4$ transition.

fluorescence intensity was at a maximum. As can be seen in Fig. 5(b), the shape of the measured resonances at magnetic field values up to several Gauss was not very sensitive to detuning. However, the contrast of the narrow nonlinear magneto-optical resonance in I_x near zero magnetic field decreased noticeably as the laser detuning was scanned from -300 to $+300$ MHz. The reason is that at larger detuning the radiation tends to excite more strongly those transitions in which the total

ground-state angular momentum F_g is less than the total excited state angular momentum F_e . Resonances at transitions with $F_g < F_e$ should be bright rather than dark [29,30]. Fig. 5(c) shows theoretical calculations for the fluorescence observed directly from the $7P_{3/2}$ state, with the assumption that the laser is tuned exactly to the frequency of the $F_g = 4 \rightarrow F_e = 4$ transition. The dark resonance that was observable in I_x in Fig. 5(b) is not apparent in the theoretical calculations. One can suppose that the exact frequency of the $F_g = 4 \rightarrow F_e = 4$ transition lies closer to the laser frequency that was detuned by $+300$ MHz from the frequency of maximum fluorescence, than to the laser frequency detuned by -300 MHz, but the calculations are too time-consuming to verify this supposition.

Fig. 6 shows the intensity versus magnetic field for two orthogonally polarized fluorescence components measured from the $6P_{3/2}$ level, which was populated from the $7P_{3/2}$ level via cascades, for various values of the laser detuning. As in the previous figure, the value of zero detuning [Fig. 6(a)] was chosen for the laser frequency that corresponded to the maximum observed fluorescence intensity. Fig. 6(b) shows the results for detunings of -375 and $+375$ MHz. It is interesting to note that at a detuning of -375 MHz a narrow dark resonance is observed in I_x , whereas at a detuning of $+375$ MHz the resonance is bright. As the detuning is increased, the transitions that are excited tend more towards transitions with $F_e > F_g$, which is the criterion for a bright resonance. Fig. 6(c) shows the results of the theoretical calculations made with the assumption that the laser is tuned exactly to the $F_g = 4 \rightarrow F_e = 4$ transition. The agreement between the curves in Fig. 6(c) and the experiment is not too good, but it is qualitatively correct. In particular, both the theoretical curve

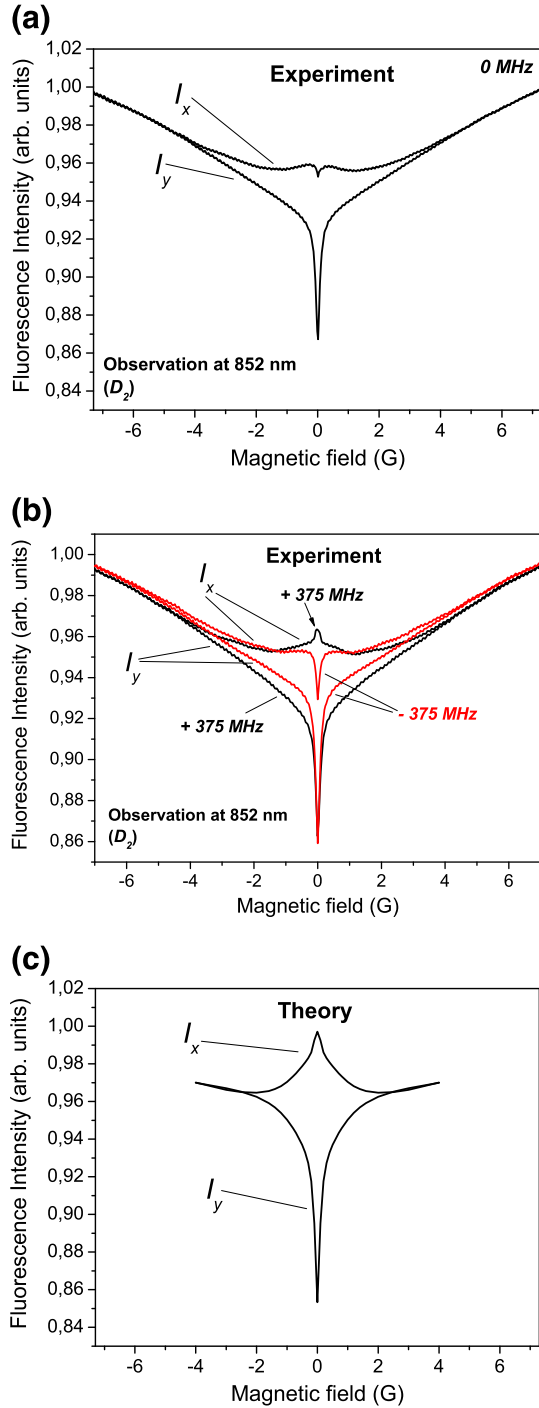


Fig. 6. Intensities of the orthogonally polarized components I_x and I_y of the fluorescence from the $6P_{3/2}$ state to the ground state (D_2) versus the magnetic field for excitation from the $F_g = 4$ ground-state level for various laser detunings from the frequency of maximum observed fluorescence intensity. (a) Observations with the exciting laser (455 nm) tuned to frequency that gave maximum fluorescence intensity. (b) Observations with the exciting laser detuned by ± 375 MHz from the frequency at which the observed fluorescence intensity was at a maximum. (c) Theoretical calculations for the laser tuned exactly to the $F_g = 4 \rightarrow F_e = 4$ transition.

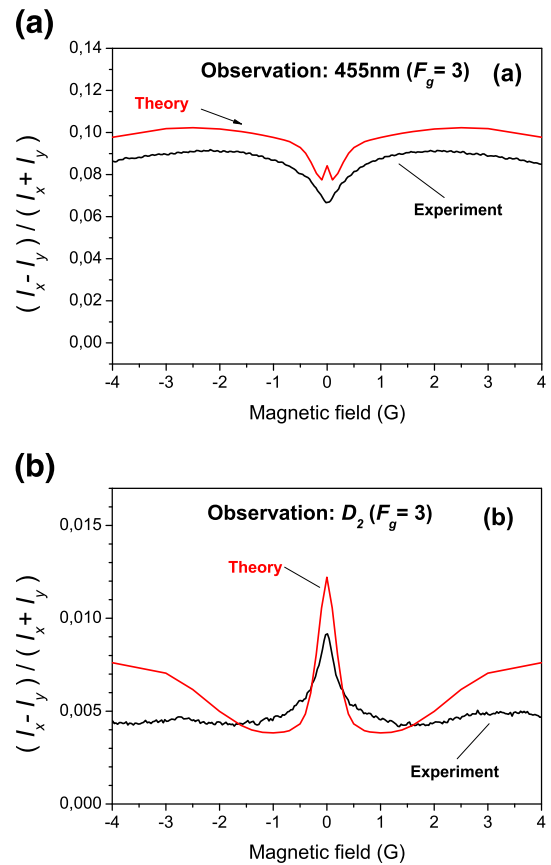


Fig. 7. Polarization degree of the fluorescence $[(I_x - I_y)/(I_x + I_y)]$ from excitation of the $7P_{3/2}$ state from the $F_g = 3$ ground-state level as a function of the magnetic field. (a) Experiment and theory for observation of the fluorescence to the ground state from the $7P_{3/2}$ state. (b) Experiment and theory for observation of the fluorescence to the ground state from the $6P_{3/2}$ state (D_2 transition) populated from above via cascade transitions.

for zero detuning and the experimental curves for detuning of +375 MHz from the frequency of maximum fluorescence show a bright resonance in I_x .

4.3. Degree of polarization of the fluorescence

The degree of polarization of the fluorescence $(I_x - I_y)/(I_x + I_y)$ is plotted as a function of the magnetic field when the $7P_{3/2}$ state was excited from the ground-state level with total angular momentum $F_g = 3$, and fluorescence was observed back to the ground state directly from the $7P_{3/2}$ state [Fig. 7(a)] or from the $6P_{3/2}$ state [Fig. 7(b)]. The agreement between theory and experiment in this case is quite good over a range of magnetic field values from -4 G to $+4$ G. However, the theoretical calculation for fluorescence from the $7P_{3/2}$ state suggests that at zero magnetic field there should have been a small feature with negative second derivative, which was not observed in the experiment.

Fig. 8 shows the polarization degree of the fluorescence as a function of magnetic field when the $7P_{3/2}$ state was excited from the $F_g = 4$ ground-state level. The results for fluorescence observed from the $7P_{3/2}$ state to the ground state are shown in Fig. 8(a), while Fig. 8(b) depicts the results for fluorescence observed from the $6P_{3/2}$ state populated from above via cascade transitions. Results from experimental observations are compared with the results of theoretical calculations. In general, the theoretical calculations qualitatively describe the experimentally measured curves, although the agreement in the contrast is not very precise. The inevitable depolarization of the experimentally measured signals was not taken into account in the theoretical calculations.

The polarization degree $(I_x - I_y)/(I_x + I_y)$ in Figs. 7 and 8 is related to the polarization moments, which appear in the multipole expansion of the density matrix (see, for example, Ref. [19]). By comparing the vertical scales of Fig. 7(a) and (b), one finds that the polarization degree observed from the $7P_{3/2}$ level was an order of magnitude higher than that observed from the $6P_{3/2}$ level when the $7P_{3/2}$ level was excited from the ground-state sublevel with $F_g = 3$ and the $6P_{3/2}$ state was populated by spontaneous cascade transitions from the $7P_{3/2}$ state through various intermediate states. It should be noted that the reduction in polarization degree depends on the external magnetic field and the shape of the plot of polarization degree versus magnetic field markedly differs in Fig. 7(a) and (b). In the case of excitation from the ground-state sublevel with $F_g = 4$, the polarization degree observed from the $6P_{3/2}$ state is also smaller than the polarization degree observed from the $7P_{3/2}$ state, but only by a factor of three. In this case, the shape of the plots in Fig. 8(a) and (b) do not differ as dramatically as in the case of excitation from the ground-state sublevel with $F_g = 3$, although the peak in Fig. 8(b) is narrower than the peak in Fig. 8(a). The reasonable agreement between experimental measurements and theoretical calculations in these figures suggests that the density matrix is well known in this system of many levels connected by spontaneous cascade transitions.

It should be noted that the transfer of polarization from one level to another has been studied theoretically in Ref. [31]. There it was shown that the maximum polarization moment rank κ of an excited state with unresolved hyperfine structure that can be observed through fluorescence is $\kappa \leq 2J_e$. In particular, this means that the polarization degree observed from the D_1 line should be zero, since a non-zero polarization degree in the fluorescence would imply a polarization rank $\kappa = 2$. In fact, we measured it to be zero at zero magnetic field and less than 0.7% over the range of magnetic field values from -7 G to 7 G.

5. Conclusion

The ground-state, nonlinear magneto-optical resonances have been observed in the fluorescence from the $7P_{3/2}$ state populated by linearly polarized 455 nm laser radiation and from the $6P_{3/2}$ and $6P_{1/2}$

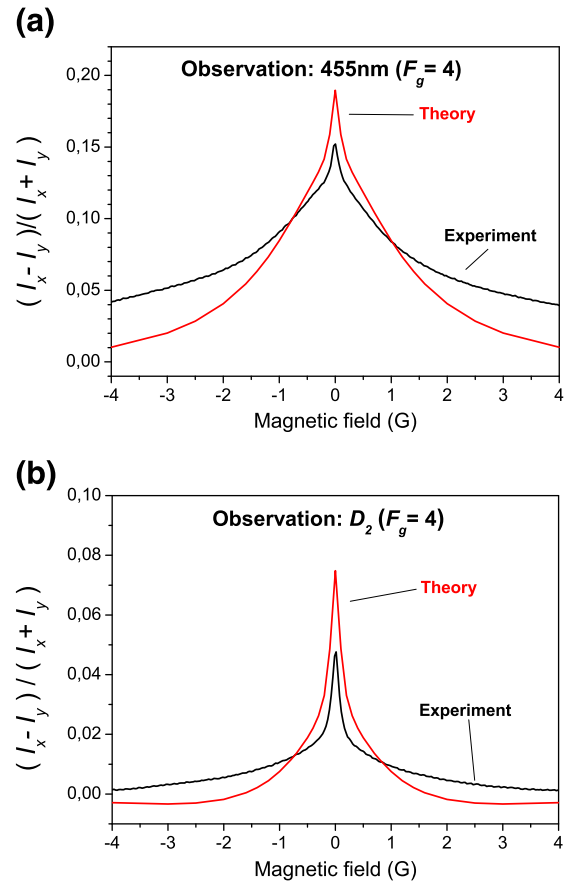


Fig. 8. Polarization degree of the fluorescence $[(I_x - I_y)/(I_x + I_y)]$ for excitation of the $7P_{3/2}$ state from the $F_g = 4$ ground-state level as a function of the magnetic field. (a) Experiment and theory for observation of the fluorescence to the ground state from the $7P_{3/2}$ state. (b) Experiment and theory for observation of the fluorescence to the ground state from the $6P_{3/2}$ state (D_2 transition) populated from above via cascade transitions.

states populated via cascade transitions from the $7P_{3/2}$ state. A theoretical description of these effects has been furnished and compared to experimentally measured signals. The theoretical model was based on an earlier model that had been developed for D -line excitation in alkali metal atoms and was based on the optical Bloch equations with averaging over the Doppler profile. This model was modified to take into account the populations of all levels, including levels populated by cascade transitions. The model also accounted for the mixing of the magnetic sublevels in an external magnetic field, which was significant in the experiment for some of the higher states with small hfs splittings. In general, the agreement between the observed signals and the calculated curves was surprisingly good, especially taking into account that the experimental parameters were only estimated.

Cascade techniques are interesting because they provide a way to observe magneto-optical resonances in fluorescence at a frequency far removed from the exciting laser radiation.

Acknowledgments

We thank Stefka Cartaleva for drawing our attention to this interesting research question and Robert Kalendarev for preparing the cesium cell. This project was carried out with support from the Latvian Science Council Grant No. LZP 09.1567 and the State Research Program Grant No. 2010/10-4/VPP-2/1 "Development of innovative multifunctional materials, signal processing and information technology for competitive, science

intensive products”, and the ESF project Nr. 2009/0223/1DP/1.1.1.2.0./09/APIA/VIAA/008. L. K. acknowledges support from the ESF project Nr. 2009/0138/1DP/1.1.2.1.2./09/APIA/VIAA/004.

References

- [1] M. Tsukakoshi, K. Shimoda, *J. Phys. Soc. Jpn* 26 (1969) 758.
- [2] C. Carrington, *J. Phys. B* 5 (1972) 1572.
- [3] B.R. Bulos, R. Gupta, W. Happer, *J. Opt. Soc. Am.* 66 (1976) 426.
- [4] C. Tai, W. Happer, R. Gupta, *Phys. Rev. A* 12 (1975) 736.
- [5] S. Chang, R. Gupta, W. Happer, *Phys. Rev. Lett.* 27 (1971) 1036.
- [6] R. Gupta, S. Chang, C. Tai, W. Happer, *Phys. Rev. Lett.* 29 (1972) 695.
- [7] J.C. Lehmann, C. Cohen-Tannoudji, *C.R. Acad. Sci. Paris* 258 (1964) 4463.
- [8] R.W. Schmieder, A. Lurio, W. Happer, A. Khadjavi, *Phys. Rev. A* 2 (1970) 1216.
- [9] G. Alzetta, A. Gozzini, L. Moi, G. Orriols, *Il Nuovo Cimento B* 36 (1976) 5.
- [10] M. Ducloy, M.P. Gorza, B. Decomps, *Opt. Commun.* 8 (1973) 21.
- [11] W. Gawlik, J. Kowalski, R. Neumann, F. Träger, *Opt. Commun.* 12 (1974) 400.
- [12] Y. Dancheva, G. Alzetta, S. Cartalava, M. Taslakov, C. Andreeva, *Opt. Commun.* 178 (2000) 103.
- [13] S. Gozzini, S. Cartaleva, T. Karulanov, A. Lucchesini, D. Slavov, *Acta Phys. Pol. A* 116 (2009) 492.
- [14] R. Gupta, S. Chang, W. Happer, *Phys. Rev. A* 6 (1972) 529.
- [15] J.L. Picqué, *J. Phys. B* 11 (1978) L59.
- [16] M. Auzinsh, R. Ferber, F. Gahbauer, A. Jarmola, L. Kalvans, *Phys. Rev. A* 78 (2008) 013417.
- [17] M. Auzinsh, R. Ferber, F. Gahbauer, A. Jarmola, L. Kalvans, *Phys. Rev. A* 79 (2009) 053404.
- [18] S. Stenholm, *Foundations of Laser Spectroscopy*, Dover Publications, Inc., Mineola, New York, 2005.
- [19] M. Auzinsh, D. Budker, S.M. Rochester, *Optically Polarized Atoms*, Oxford University Press, Oxford, 2010.
- [20] M. Auzinsh, R. Ferber, *Optical Polarization of Molecules*, 2nd edition, Cambridge University Press, Cambridge, 2005.
- [21] K. Blushs, M. Auzinsh, *Phys. Rev. A* 69 (2004) 063806.
- [22] D.A. Steck, *Cesium D line data*, 2003.
- [23] E. Arimondo, M. Inguscio, P. Violino, *Rev. Mod. Phys.* 49 (1977) 31.
- [24] C.E. Theodosiou, *Phys. Rev. A* 30 (1984) 2881.
- [25] K.B. Eriksson, I. Johansson, G. Norlen, *Ark. Fys.* 28 (1964) 233.
- [26] H. Kleiman, *J. Opt. Soc. Am.* 52 (1962) 441.
- [27] R.L. Kurucz, B. Bell, *Atomic Line Data*, CD-ROM No. 23, Smithsonian Astrophysical Observatory, Cambridge, MA (1995).
- [28] J. Alnis, K. Blushs, M. Auzinsh, S. Kennedy, N. Shafer-Ray, E.R.I. Abraham, *J. Phys. B* 36 (2003) 1161.
- [29] F. Renzoni, S. Cartaleva, G. Alzetta, E. Arimondo, *Phys. Rev. A* 63 (2001) 065401.
- [30] J. Alnis, M. Auzinsh, *J. Phys. B* 34 (2001) 3889.
- [31] M. Auzinsh, D. Budker, S.M. Rochester, *Phys. Rev. A* 80 (2009) 053406.